Lawrence Berkeley National Laboratory

The Impact of Evaporation Process on Thermal Performance of Roofs - Model Development and Numerical Analysis

Lei Zhang, Ronpeng Zhang, Yu Zhang, Tianzhen Hong, Qinglin Meng & Yanshan Feng

Lawrence Berkeley National Laboratory

Disclaimer:

The Impact of Evaporation Process on Thermal Performance of Roofs - Model Development and Numerical Analysis

Lei Zhang[1, 2], Rongpeng Zhang[2], Yu Zhang[3,2], Tianzhen Hong[2],Qinglin Meng[1], Yanshan Feng[1]

1. Building Energy and Environment Laboratory, School of Architecture, Guangzhou Municipal Key Laboratory of Landscape Architecture, State Key Lab of Subtropical Building Science, South China University of Technology, Wushan Road, Tianhe District, Guangzhou 510641, P.R.China.

2. Building Technology and Urban Systems Division, Lawrence Berkeley National Laboratory, Berkeley, CA 94720, USA

3. School of Chemistry and Chemical Engineering, South China University of Technology, Wushan Road, Tianhe District, Guangzhou 510641, P.R.China.

Abstract: This article presented a methodology for modeling and analyzing the influence of evaporation process on thermal performance of roofs. Based on the experimental data in a climatic wind tunnel, a mathematical model was developed to predict the hourly evaporation amount using multivariate nonlinear regression analysis. Then, the model was adopted to calculate the boundary conditions of a roof surface, which was further applied to estimate surface temperature and heat flux of the roof using finite difference method. Finally, the impact of evaporation process, including the evaporation starting time and water replenishing frequency, on the roof thermal performance was analyzed. The results indicated that when evaporation commenced at 11:00, compared to the corresponding value of no-evaporation roof, the highest external surface temperature was reduced by 1.8°C; the accumulated internal surface heat flux from 16:00-20:00 was decreased by 10.8% which could be doubled to 21.2% if the evaporation layer was replenished water frequently.

1 Introduction

Net Zero Energy Building (NZEB) is no longer a distant concept but rather a practical solution to mitigate CO_2 emissions and/or decrease energy consumption in buildings [1]. Goals for the implementation of NZEBs are discussed at the international level. In the USA, the Energy Independence and Security Act of 2007 authorized the Net-Zero Energy Commercial Building Initiative to support the goal of net zero energy for all new commercial buildings by 2030. It further specified a zero-energy target for 50% of U.S. commercial buildings by 2040 and net zero for all U.S. commercial buildings by 2050. At the European region, the Energy Performance of Buildings Directive establishes the nearly zero energy building as the building target from 2018 for all buildings public owned or occupied and from 2020 for all new buildings [1]. Some similar promotions or plans are also presented in the China, UK, Canada, Japan, Korea and Australia [2-3].

In order to achieve the NZEB objectives, two main strategies could be applied in the design and operation of buildings: (a) reduce the energy demand of the buildings to the highest extent, and (b) supply the remaining energy demand through on-site renewable energy sources [4]. The former can be achieved by either active or passive energy efficient strategies. Instead of the conventional active building environmental control approaches that solely rely on the mechanical air conditioning systems, increasing attention is given to the passive strategies for their exceptional environmental performance [5].

Evaporative cooling is one of the passive building energy efficiency strategies. After being

2

absorbed in porous materials, the water in the pores gradually migrates to the surface layer of the material and evaporates under the combined effect of natural climate elements such as solar radiation, air temperature, humidity, and wind speed; this would result in a cooling effect to the surrounding environment and reduce the urban heat island intensity and building energy consumption [6]. The effectiveness of evaporative cooling has been proved in different climatic situations, not only on hot and dry regions [7-9] where it was initially applied but also in hot and humid ones[10-12].

In the previous study, most researchers investigated evaporative cooling at the material level using measurement data. Wanphen et al. [13] measured the moisture and thermal performance of a number of porous materials, including pebbles, silica sand, volcanic ash, and siliceous shale. It was found that the daily average surface temperature can be reduced by up to 8.6℃. Pires et al. [14] studied the evaporative cooling capability of five types of textile fabrics in a small wind tunnel. Some other scholars focused on the optimization of material properties to enhance the evaporative cooling effects. He et al. and Chen et al. developed a passive evaporative cooling wall (PECW) constructed of moist void bricks [15] or pipe-shaped porous ceramics [16-17] that were capable of absorbing water and allowed wind penetration, thus reducing their surface temperatures by means of water evaporation. Karamanis et al. [18] optimized the selection and preparation of the porous materials using the Kelvin equation, and validated the optimization via solar-heat transformation experiments. However, there was little information available in literature about the quantified effect of realistic evaporative cooling products on the building envelope thermal performance, which may be the most critical information for building designers and owners. This may limit the application of such technology in realistic cases.

The purpose of this article is to study a roof product which is composed of evaporative cooling material and quantitatively investigate the impact of the evaporation process on the roof thermal performance. Firstly, we developed a mathematical model to calculate the evaporation rate. Then, the model was adopted to calculate the boundary conditions of a roof surface, which was further applied to estimate surface temperature and heat flux of the roof using finite difference method. Finally, the impact of evaporation process, including the evaporation starting time and water replenishing frequency, on the roof thermal performance was analyzed.

2 Roof with porous material for evaporative cooling

The roof we studied is composed of porous face brick, waterproof mortar, and concrete. The dimension of the porous face brick is 240 mm (length) ×50 mm (width) ×10 mm (thickness) and the surface solar absorptivity is 0.76 [11].

In our previous article [11], we measured the mass moisture content variation of the porous face brick with respect to the soaking time. According to the measurement data, after one hour of soaking in water, the mass moisture content is 7.49%.

The evaporation process in porous face brick could be divided into three stages: a constant-rate stage, a falling-rate stage, and a low-rate stage. Within the first stage, the evaporation rate is determined by the available energy (radiation) and atmospheric conditions (vapor pressure, wind velocity, etc.). During the second and third stages, evaporation rate is jointly controlled by the water, energy supply, and atmospheric conditions. The evaporation amount within the first stage is much higher than that within the second and third stages. Therefore, we defined the mass moisture content at the turning point between the first stage and the second stage as the critical mass moisture content, below which the evaporation process was ignored. The critical mass moisture

content of the porous face brick is 3.1% [11].

The thermal resistance of each material layer, which was calculated according to the thermodynamic parameters of the materials, is shown in Table 1. The combined heat transfer coefficients at the external and internal surfaces are assumed to be 22 W/m^2·K and 9 W/m^2·K [19], respectively.

Table 1 The thermal resistance of each material layer [20].

Description (from outside to inside)	Thickness d (mm)	Thermal conductivity λ (W/m·K)	Density ρ (kg/m^3)	Specific heat c (kJ/kg·K)	Thermal resistance R=d/λ (m^2·K/W)
Porous face brick	10	0.24	1654	0.43	0.012
Waterproof mortar	10	0.93	1800	1.05	0.011
Concrete	180	1.28	2100	0.92	0.141

3 Mathematical model of evaporation rate

The evaporation amount is one of the key parameters to evaluate the evaporation heat exchange on the wet surface. Recently researchers successfully introduced the Penman-Monteith (P-M) equation, which was initially applied to calculate soil evaporation rate in Pedology field, to estimate the evaporation amount of wet building porous materials [12, 21].

It can be seen from Eq. (1) that the independent variables in P-M equation included solar radiation, ambient air temperature, relative humidity, wind velocity, and surface heat flux.

$$E = \frac{c_1\Delta(R_n - G)}{\Delta + \gamma(1 + a_3 u)} + \frac{c_2 \dfrac{\gamma}{T + 273}u(e_s - e_a)}{\Delta + \gamma(1 + c_3 u)} \tag{1}$$

During the building energy simulation process, the solar radiation, ambient air temperature,

relative humidity, and wind velocity could be conveniently accessed from the typical

meteorological year data. While the surface heat flux is obtained through the surface heat balance

and building envelope heat transfer calculation. Additionally, the surface heat flux interacted with

evaporating process, so only after multiple iterations is it possible to get the correct results. It is

necessary to reasonably simplify the evaporation amount calculation during the building energy

simulation process. In our previous article [?], using a climatic wind tunnel we measured the

independent variables of the P-M equation and then obtained the hourly evaporation amount [12].

Based on the experimental data, the following regression analysis was conducted in this article.

Firstly, the unitary regression equations between the four individual independent variables and

evaporation amount were established. Secondly, the multivariate nonlinear regression model was

proposed based on the four unitary regression equations. In the end, the OriginPro software [?]

was adopted to regress the coefficients in the model.

The unitary regression equations between the four individual independent variables and

evaporation amount are shown in Fig. 1. The significant linear relationship (R^2=0.9803) between

hourly evaporation amount and surface net shortwave radiation could be observed in Fig. 1(a). If

the linear regression equation was used to predict the evaporation amount, when the surface net

shortwave radiation is zero, the evaporation rate is constant and equal to 0.02 kg/m^2·h. But

according to the P-M equation, when the surface net shortwave radiation is zero, evaporation rate

varies with the water vapour partial pressure difference between wet surface and ambient air. Thus,

in addition to the surface net shortwave radiation, three other independent variables should be

considered, i.e. ambient air temperature, relative humidity, and wind velocity. As shown in

Fig.1(b)-(d), exponential functions were introduced to describe the nonlinear regression equations

6

between the three individual independent variables and evaporation rate. To model the comprehensive influence of the radiation term and the aerodynamic term, we developed a multivariate nonlinear regression model as shown in Eq. (2)

$$E_a = a_1 \cdot x_1 + e^{\left(a_2 + \frac{a_3}{x_2 + a_4}\right)} + e^{\left(a_5 + a_6 \cdot x_3 + a_7 \cdot x_3^2\right)} + e^{\left(a_8 + \frac{a_9}{x_4 + a_{10}}\right)} + a_{11} \tag{2}$$

Where, a_1 - a_{11} are regression model coefficients, x_1 - x_4 are the surface net shortwave radiation, ambient air temperature, relative humidity, and wind velocity.
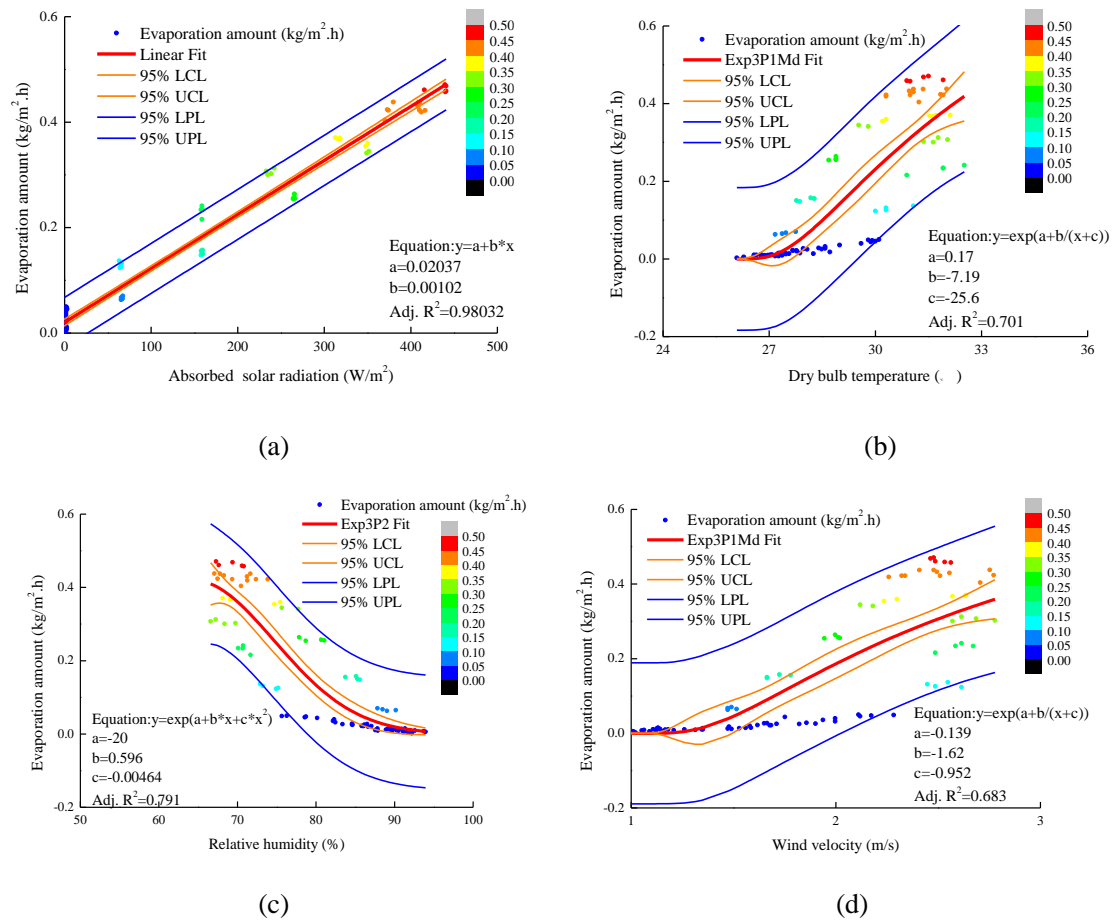
(a)Evaporation amount vs. Absorbed solar radiation. (b) Evaporation amount vs. Dry bulb temperature. (c) Evaporation amount vs. Relative humidity. (d) Evaporation amount vs. Wind velocity

Fig.1 The relationships among impact factors and evaporation amount

The value of a_1 - a_{11} were obtained by regression analysis using the software OriginPro and

the mathematical model for calculating the evaporation amount is shown in Eq. (3):

$$E_a = 0.000842 \cdot q_s + e^{1.45-\frac{77.2}{t_a-14.4}} + e^{1.3 \cdot R_h - 0.01 \cdot R_h^2 - 45.6} + e^{-1.2-\frac{7.24}{v+0.355}} - 0.00399 \qquad (3)$$

The variation range of the independence variables in Eq. (6) is shown in Table 2.

Table 2 The range of the independence variables

	Minimum value	Maximum value	Average value	Standard deviation
q_s (W/m^2)	0	440.73	136.09	163.57
t_a (°C)	26.09	32.51	29.04	1.90
R_h (%)	66.59	93.94	81.00	8.96
v (m/s)	0.95	2.78	1.89	0.58

The adjust R square of the model is 0.99973 and the F test is highly significant (F= 60465，P<0.001). Furthermore, histogram of standardized residuals is plotted in Fig. 2 from which one can see that the distribution of standardized residuals follows a normal distribution. In addition, Fig.3 plots the distribution of residuals between measured evaporation rates and the predicted values, which shows that (1) the distribution of the predicted evaporation rate is close to the profile of measured values, (2) the absolute values of the residuals do not exceed 0.009 kg/m^2·h, and (3) the variation range of the residuals is approximately constant with different measured evaporation amount which demonstrated that the residuals was homoscedasticity.
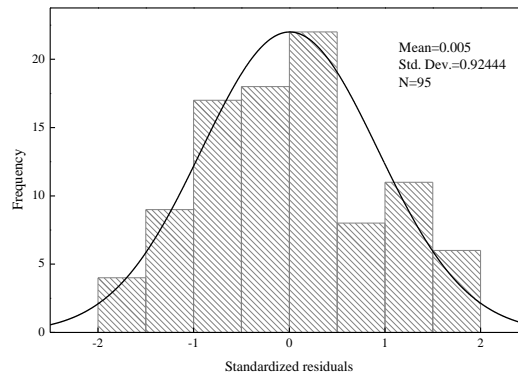

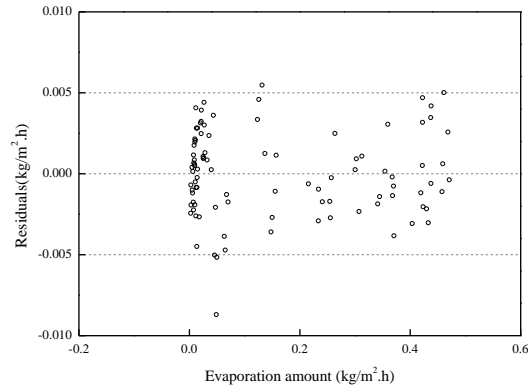Fig.2 Histogram of standardized residuals

Fig.3 Residual distribution of measured value and predicted value of evaporation

Based on the above tests, we can conclude that the mathematical model of evaporation rate obtained by the regression method is a statistically significant model with a practical value and high reliability that can therefore be used to estimate variations in the hourly evaporation rate.

4 Numerical analysis of thermal performance of roofs

4.1 One-dimensional unsteady heat transfer

A procedure for periodic solution of unsteady heat flow problem for the composite roof is presented in this section. Schematic representation of the roof is indicated in Fig. 4. The roof structure comprises of three material layers, and thickness of the layers are L1, L2, and L3, respectively.

Depending on physical situation of the structures, solution of the problem was performed under these assumptions: a) no internal heat generation in any material layer of roofs, b) homogeneity of each layer of structures with fixed thermo-physical properties, c) resistance of the layer interface was neglected assuming good contact of the material layers.

In accordance with the above-mentioned assumption, the governing equation and the boundary condition are developed as below.
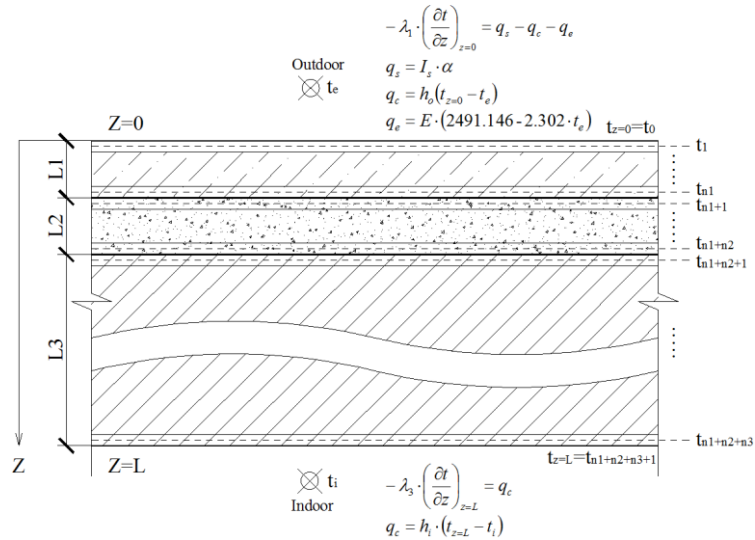
Fig.4 Schematic representation of the roof

Governing Equation:

$$\frac{\partial t}{\partial \tau} = \frac{\lambda}{\rho \cdot c} \cdot \frac{\partial^2 t}{\partial z^2} \qquad\qquad [0 < z < L]$$

(4)

The same equation held good for all the three material regions by incorporating suitable λ, ρ,

c value. In the external boundary ($z = 0$) where the roof was exposed to solar radiation, the

boundary condition is:

$$-\lambda_1 \cdot \left(\frac{\partial t}{\partial z}\right)_{z=0} = q_s - q_c - q_e \qquad\qquad (5)$$

where, $q_s = I_s \cdot \alpha$, $q_c = h_o \cdot (t_{z=0} - t_e)$, $q_e = E \cdot (2491.146 - 2.302 \cdot t_e)$.

When discussing the surface heat balance equation, most previous studies have only considered

the solar radiation term and the combined convection and radiation heat transfer term [22-23]. In

this article, the evaporative heat transfer term, which was calculated by using the mathematical

model in section 3, was taken into account.

In the bottom layer of the concrete slab z = L, the boundary condition is:

10

$$-\lambda_3 \cdot \left(\frac{\partial t}{\partial z}\right)_{z=L} = q_c \tag{6}$$

where, $q_c = h_i \cdot (t_{z=L} - t_i)$

The instantaneous continuity of heat flux and temperature at the interfaces Z = L1 and L2 are preserved.

The derivative $\frac{\partial t}{\partial \tau}$, $\frac{\partial t}{\partial z}$, and $\frac{\partial^2 t}{\partial z^2}$, as shown in Eqs. (7), were approximated by the following difference scheme, respectively.

$$\frac{\partial t_k}{\partial z} \approx \frac{t_k^m - t_{k-1}^m}{(\Delta z_{k-1} + \Delta z_k)/2} \tag{7}$$

$$\frac{\partial t_{k+1}}{\partial z} \approx \frac{t_{k+1}^m - t_k^m}{(\Delta z_k + \Delta z_{k+1})/2} \tag{8}$$

$$\frac{\partial^2 t_k}{\partial z^2} = \frac{\partial(\partial t_k/\partial z)}{\partial z} \approx \left[\frac{t_{k+1}^m - t_k^m}{(\Delta z_{k+1} + \Delta z_k)/2} - \frac{t_k^m - t_{k-1}^m}{(\Delta z_k + \Delta z_{k-1})/2}\right]\Big/\Delta z_k \tag{9}$$

$$\frac{\partial t_k}{\partial \tau} \approx \frac{t_k^m - t_k^{m-1}}{\Delta \tau} \tag{10}$$

The equation for the top volume cell is rewritten as below.

$$\left(1 + \frac{\lambda_1}{\Delta z_1 \cdot h_o}\right)t_0^m + \left(-\frac{\lambda_1}{\Delta z_1 \cdot h_o}\right)t_1^m = t_{sol-air}^m \tag{11}$$

$$t_{sol-air}^m = t_e^m + \frac{q_s(m)}{h_o} - \frac{q_e(m)}{h_o} \tag{12}$$

In our model, the boundary conditions are limited to Fourier type in a linear form. Consequently, the sol-air temperature [22-23] approach was used in this article to describe the equivalent outdoor air temperature that gives the same rate of heat flow to a surface as would the combination of incident solar radiation, convection with the ambient air, and radiation exchange with the surrounding surfaces, and evaporative heat transfer.

The equation for the bottom volume cell is rewritten as below.

$$\left(-\frac{\lambda_3}{\Delta z_3 \cdot h_i}\right) t^m_{n1+n2+n3} + \left(1+\frac{\lambda_3}{\Delta z_3 \cdot h_i}\right) t^m_{n1+n2+n3+1} = t^m_i \qquad (13)$$

The equation for any volume cell that is located in between the top and bottom volume cells of

a particular material is rewritten as below.

$$\left(-\gamma_D\right) t^m_{k-1} + \left(1+2\gamma_D\right) t^m_k + \left(-\gamma_D\right) t^m_{k+1} = t^{m-1}_k \qquad (14)$$

$$\gamma_D = \frac{\lambda_D \cdot \Delta\tau}{c_D \cdot \rho_D \cdot \Delta z_D^2} \qquad (15)$$

The above-mentioned discretized equations were not applicable for volume cells n1, n1+1,

n1+n2, n1+n2+1, due to these cells were interface nodes of two different layers.

The equation for the volume cell n1 is rewritten as below:

$$\left(-\gamma_1\right) \cdot t^m_{k-1} + \left(1+\gamma_1+\gamma_{1,2}\right) \cdot t^m_k + \left(-\gamma_{1,2}\right) \cdot t^m_{k+1} = t^{m-1}_k \qquad (16)$$

$$\gamma_1 = \frac{\lambda_1 \cdot \Delta\tau}{c_1 \cdot \rho_1 \cdot \Delta z_1^2}, \gamma_{1,2} = \frac{2 \cdot \lambda_{1,2} \cdot \Delta\tau}{c_{1,2} \cdot \rho_{1,2} \cdot \Delta z_1 \cdot \left(\Delta z_1 + \Delta z_2\right)}$$

where, $\lambda_{1,2} = \dfrac{\Delta z_1 + \Delta z_2}{\dfrac{\Delta z_1}{\lambda_1} + \dfrac{\Delta z_2}{\lambda_2}}$, $\rho_{1,2} = \dfrac{\rho_1 \cdot \Delta z_1 + \rho_2 \cdot \Delta z_2}{\Delta z_1 + \Delta z_2}$, $c_{1,2} = \dfrac{c_1 \cdot \Delta z_1 + c_2 \cdot \Delta z_2}{\Delta z_1 + \Delta z_2}$

The equation for the volume cell n1+1 is rewritten as below:

$$\left(-\gamma_{2,1}\right) \cdot t^m_{k-1} + \left(1+\gamma_{2,1}+\gamma_2\right) \cdot t^m_k + \left(-\gamma_2\right) \cdot t^m_{k+1} = t^{m-1}_k \qquad (17)$$

$$\gamma_2 = \frac{\lambda_2 \cdot \Delta\tau}{c_2 \cdot \rho_2 \cdot \Delta z_2^2}, \gamma_{2,1} = \frac{2 \cdot \lambda_{1,2} \cdot \Delta\tau}{c_{1,2} \cdot \rho_{1,2} \cdot \Delta z_2 \cdot \left(\Delta z_1 + \Delta z_2\right)}$$

The equation for the volume cell n1+n2 is rewritten as below:

$$\left(-\gamma_2\right) \cdot t^m_{k-1} + \left(1+\gamma_2+\gamma_{2,3}\right) \cdot t^m_k + \left(-\gamma_{2,3}\right) \cdot t^m_{k+1} = t^{m-1}_k \qquad (18)$$

$$\gamma_{2,3} = \frac{2 \cdot \lambda_{2,3} \cdot \Delta\tau}{c_{2,3} \cdot \rho_{2,3} \cdot \Delta z_2 \cdot \left(\Delta z_2 + \Delta z_3\right)}$$

$$\lambda_{2,3} = \frac{\Delta z_2 + \Delta z_3}{\dfrac{\Delta z_2}{\lambda_2} + \dfrac{\Delta z_3}{\lambda_3}} \ , \quad \rho_{2,3} = \frac{\rho_2 \cdot \Delta z_2 + \rho_3 \cdot \Delta z_3}{\Delta z_2 + \Delta z_3} \ , \quad c_{2,3} = \frac{c_2 \cdot \Delta z_2 + c_3 \cdot \Delta z_3}{\Delta z_2 + \Delta z_3}$$

The equation for the volume cell n1+n2+1 is rewritten as below:

$$\left(-\gamma_{3,2}\right) \cdot t_{k-1}^m + \left(1 + \gamma_{3,2} + \gamma_3\right) \cdot t_k^m + \left(-\gamma_3\right) \cdot t_{k+1}^m = t_k^{m-1} \tag{19}$$

$$\gamma_3 = \frac{\lambda_3 \cdot \Delta\tau}{c_3 \cdot \rho_3 \cdot \Delta z_3^2} , \gamma_{3,2} = \frac{2 \cdot \lambda_{2,3} \cdot \Delta\tau}{c_{2,3} \cdot \rho_{2,3} \cdot \Delta z_3 \cdot \left(\Delta z_2 + \Delta z_3\right)}$$

The governing equations along with the boundary conditions were discretized using semi-implicit control volume formulation. A time step of half an hour was used within the simulation. The system of equations was solved using tridiagonal matrix algorithm (TDMA). The initial temperature values were obtained by executing the program, continuously for a few days till the routine daily variation attained the same value.

Based on the numerical model mentioned above, a computer program was developed in Visual Basic to implement the roof thermal performance analysis. The program was validated against a study case derived from previously published work by Kaşka, Ö., and Yumrutaş, R [19], in which a site measurement for a specific roof was conducted. The roof has 2 cm plaster at the inside surface of the concrete roof with thickness of 12 cm. Thermophysical properties of the roof materials are listed in Table 3. The inside design air temperature and roof surface solar absorptivity are taken to be 25 °C and 0.8, respectively. The combined heat transfer coefficients at the internal and external surfaces are taken to be 9 and 22 W/m^2·$^{\text{o}}$C, respectively [19].

Table 3 Thermophysical properties of the roof materials [19]

Materials	Thermal conductivity (W/m·K)	Density (kg/m^3)	Specific heat (J/kg·K)
Plaster	0.700	2778	840
Concrete	1.730	2400	840

Fig. 5 shows the daily variation of measured and calculated surface temperatures and heat flow through the roof structure.
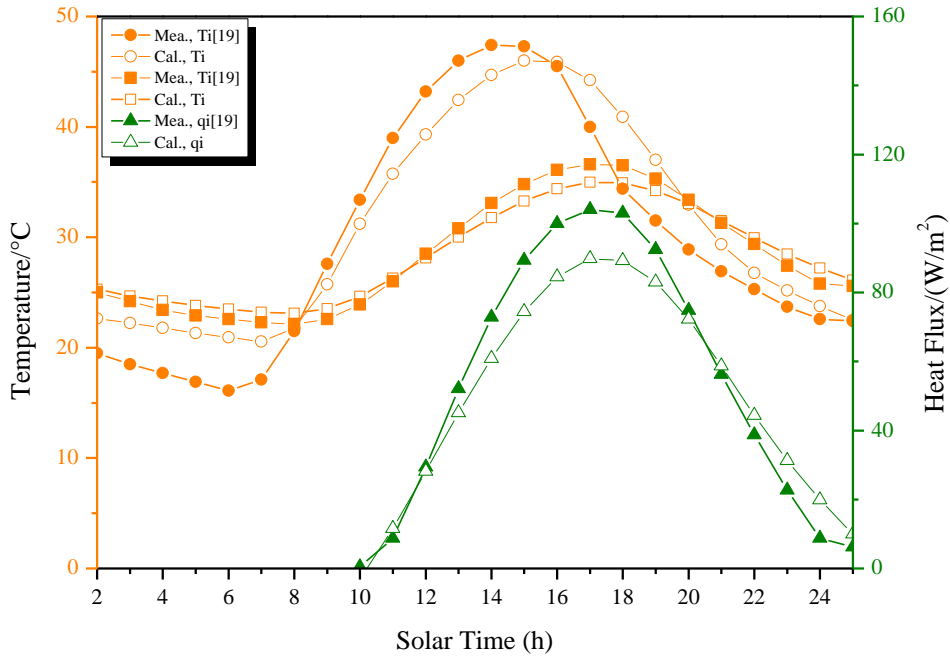
Fig.5 Variation of heat flux and surface temperature of roof construction

It is observed from the results that the computer program is verified. Since values of temperatures obtained from the computer program in this article are close to the measured values in literature [19] with a finite error. The mean relative error between calculated and measured surface temperature are found to be 11.3% (external surface) and 3.2% (internal surface), respectively. So the computer program was used to carry out the following roof thermal performance analysis.

4.2 Roof thermal performance under various evaporation conditions

In this article, the influence of the evaporation starting time and water replenishing frequency on the roof thermal performance were analyzed since these two factors considerably affected the evaporation process.

The analysis will be limited to the calculation of the external surface temperature and the internal surface heat flux of the roof because they have significant influence on the outdoor thermal environment and indoor cooling load.

The Typical Meteorological Day of Guangzhou, China was adopted as the periodic outdoor signal [12], as shown in Fig. 6. The indoor air temperature was set to a constant value i.e. 22 °C. Other boundary conditions, including surface solar absorptivity, thermal resistance of each layer,

14

and combined heat transfer coefficients at the external and internal surfaces were listed in section
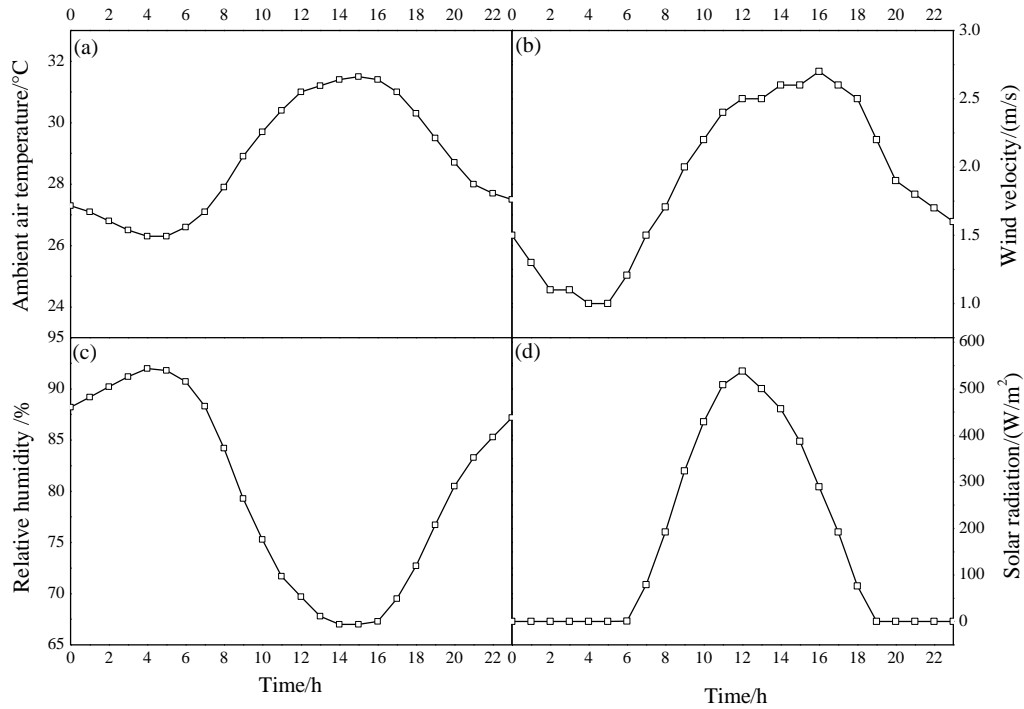
2.

Fig.6 Periodic outdoor signal

The thermal conductivity, specific heat capacity, and density of the porous face brick would be changed when it absorbed water. In this article, the thickness of the porous brick was only 10 mm while the thickness of the concrete layer was 180 mm, so the error caused by the variation of the thermophysical properties was relatively small. Therefore, the variation of the thermal conductivity, specific heat capacity, and density of the porous face brick were ignored in the calculation of roof one-dimensional unsteady heat transfer.

4.2.1 Evaporation started at different time of day

Different evaporation starting times correspond to different solar radiation intensities in outdoor environments, which can therefore result in varying of evaporation heat transfer and consequently affect the roof thermal performance. To analyse the effect of the evaporation starting time on the roof thermal performance, we calculated variation trends of the external surface temperature and the internal surface heat flux of the roof when evaporation started at 7:00, 11:00, and 15:00. The results are shown in Fig. 7.
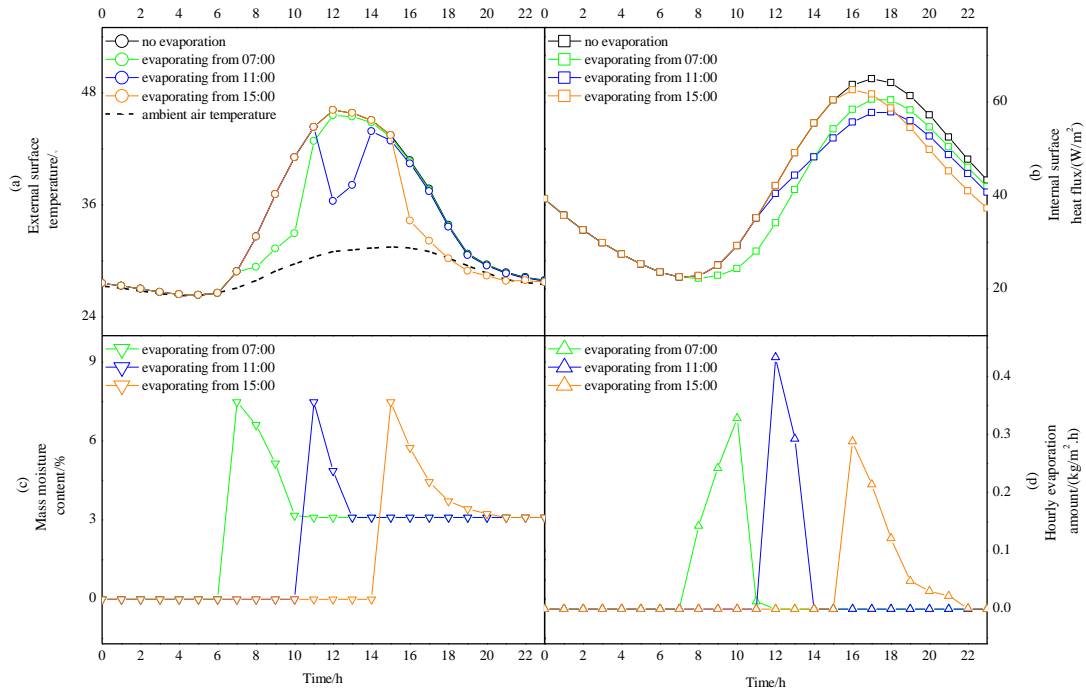
Fig.7 Impact of evaporation starting time on roof thermal performance

Taking the case of the evaporation starting time at 7:00 as an example. After the water replenishment process that occurred one hour earlier (6:01-7:00), the mass moisture content of the evaporation layer at 7:00 is 7.49%, as shown in 10(c). During the evaporation process, the mass moisture content of the evaporation layer gradually decreases. At 10:00, the mass moisture content of the evaporation layer is 3.2%, close to the critical mass moisture content of 3.1%, and the evaporation process during 10:01-11:00 is relatively weak. At 11:00, because the mass moisture content of the evaporation layer is equal to the critical mass moisture content, evaporation amount during 11:01-12:00 is approximately zero over this entire time period. Thus, the mass moisture content of the evaporation layer after 11:00 stays at 3.1%. The variation of evaporation amount in Fig. 7(d) corresponds to the mass moisture content variation in Fig. 7(c). After evaporation starts at 7:00, the evaporation amount continues to increase with gradually increasing solar radiation intensity. During 9:01-10:00, the evaporation amount reaches its maximum value in this case, which is 0.33 kg/m^2·h. After 11:00, the mass moisture content of the evaporation layer is equal to the critical mass moisture content, and the evaporation amount is therefore zero. The variation in the evaporation amount directly affects the evaporation heat transfer and therefore the roof external surface temperature. The external surface temperature variation curve in Fig. 7(a) shows that prior to the water replenishment process, the external surface temperature of the evaporative

16

cooling roof equals that of the no-evaporative roof. After the evaporation process starts, with increasing solar radiation, the evaporation amount gradually increases and the corresponding evaporation heat transfer consumes most of the solar radiation, resulting in a slow increase in the external surface temperature of the evaporative cooling roof. At 10:00, the evaporation amount reaches its maximum, and the external surface temperature of the evaporative cooling roof is lower than that of the no-evaporative roof by 8.2 °C. At 12:00, because the mass moisture content of the evaporation layer reaches the critical mass moisture content, the evaporation process weakens and the effect of evaporative cooling is suppressed. Consequently, the external surface temperature significantly increases and reaches 45.6 °C. The internal surface heat flux of the evaporative cooling roof is lower than that of the no-evaporative roof once evaporation starts. At 12:00, the internal surface heat flux difference between the evaporative cooling roof and the no-evaporative roof reaches its maximum value of 8.0 W/m^2. At 17:00, the internal surface heat flux of the evaporative cooling roof reaches its maximum value of 60.6 W/m^2.

In the cases of the evaporation starting times at 11:00 and 15:00, variations in the external surface temperature and internal surface heat flux of the evaporative cooling roof are similar to that of the case at 7:00. However, because of delayed evaporation starting time and differences in the continuous evaporation period and the time when the maximum evaporation is reached, differences arise in the average decrease of the external surface temperature and the accumulated decease of the internal surface heat flux, which are shown in Table 4.

Table 4 Average decrease of external surface temperature and accumulated decrease of internal surface heat flux

Evaporation starting time	Average decrease of external surface temperature (°C)			Accumulated decrease of internal surface heat flux (W/m^2)		
	6:00-11:00	12:00-18:00	19:00-23:00	6:00-11:00	12:00-18:00	19:00-23:00
07:00	3.1	0.3	0.06	14.7	42.7	10.9
11:00	0.0	2.9	0.1	0.0	43.5	19.3
15:00	0.0	2.2	0.9	0.0	9.8	34.4

In the daytime (6:00-18:00), solar radiation is intensity, and cooling caused by evaporation is

significant. Thus, the average decrease of the external surface temperature of the evaporative cooling roof during daytime is higher than that during night-time(19:00-23:00). Consider the case of the evaporation starting time at 11:00 as an example: because no evaporation occurs before 11:00, the average decrease in the external surface temperature is 0°C. During 12:00-18:00, due to the intensity solar radiation, cooling caused by evaporation is significant, and the average decrease in the external surface temperature is 2.9 °C. In contrast, during 19:00-23:00, the external surface temperature of the evaporative cooling roof is only 0.1°C lower than that of the no-evaporative roof.

In addition, in the case of the evaporation starting time of 7:00, the average external surface temperature during 6:00-11:00 can be significantly decreased by 3.1 °C. Because the evaporation amount at 12:00 is close to zero in this case, the surface temperature is significantly increased during the high-temperature period from 12:00 to 18:00. Although it is still lower than the external surface temperature of the no-evaporation roof, the average decrease is only 0.3 °C. In the case of the evaporation starting time of 15:00, the external surface temperatures before evaporation equal those of the no-evaporative roof. After evaporation starts, the average decrease in the external surface temperature during 12:00-18:00 is significant: 2.2 °C.

Evaporation that starts when the solar radiation is intensity can consume most of the solar radiation, thus reducing the internal surface heat flux. According to the calculations in this study, evaporation starting at 11:00 can reduce the internal surface heat flux considerably during 12:00-18:00. Compared to the internal surface heat flux of the no-evaporative roof during the same time period, evaporation starting at 11:00 can reduce the internal surface heat flux by 43.5 W/m^2, which in turn can significantly reduce the heat flux from the roof to the indoor environment and then decrease the energy consumption of air conditioners.

4.2.2 Evaporation with different water replenishing frequency

When the mass moisture content of the evaporation layer reaches the critical mass moisture content, the evaporation process is suppressed. Thus, the evaporation layer needs to be replenished with water so that evaporation can continue to cool the roof. In this study, we compared the effects of two conditions with the same evaporation starting time (11:00) on the external surface temperature and internal surface heat flux: the first condition is a single water replenishment event (i.e., after evaporation starts at 11:00, there is no water replenishment), and the second condition is

multiple water replenishment events (i.e., when the mass moisture content of the evaporation layer reaches the critical mass moisture content, water is replenished). The calculation results are shown in Fig. 8.
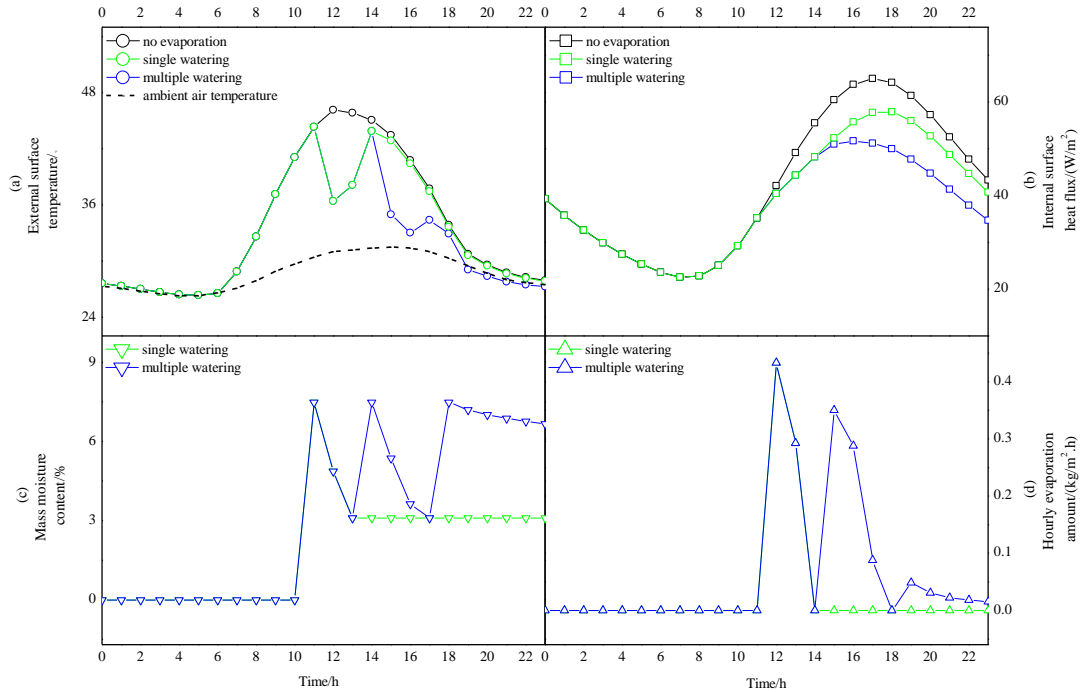

Fig.8 Impact of water replenishing frequency on roof thermal performance

Fig.8(a) shows that in the case of multiple water replenishment, the external surface temperature variation trend of the roof after the first water replenishment is similar to the case of single water replenishment. Until the mass moisture content of the evaporation layer reaches the critical mass moisture content at 13:00, water is replenished for the second time at 13:01-14:00. Evaporation resumes at 14:00. During the evaporation process over the following three hours, the surface temperature is still significantly lower than those of the no-evaporation roof and single water-replenishment roof. After the third water replenishment at 17:01-18:00, evaporation resumes again.

Fig. 8(b) shows that the internal surface heat flux in the case of multiple water replenishment is significantly lower than that of the no-evaporation roof and single water-replenishment roof. At 16:00, the internal surface heat flux in the case of multiple water replenishment reaches the maximum value, 51.7 W/m^2, which is lower by 6.2 W/m^2 with respect to the maximum value of the internal surface heat flux in the case of single water replenishment.

Fig. 8(c) and (d) describe the mass moisture content and corresponding evaporation amount

profiles of the evaporation layer in the cases of single and multiple water replenishment. For single water replenishment, when the mass moisture content of the evaporation layer reaches the critical mass moisture content, it is assumed that evaporation ceases and the evaporation amount is therefore zero. In the case of multiple water replenishment, when the mass moisture content reaches the critical mass moisture content, water replenishment starts and the mass moisture content of the evaporation layer increases to the level of the initial mass moisture content; evaporation then resumes and the mass moisture content of the evaporation layer gradually decreases. When the mass moisture content reaches the critical mass moisture content again, this whole process is repeated.

The average decreases in the external roof surface temperature and the accumulated heat flux of the inner surface for these two water replenishment conditions are shown in Table 5. As can be observed, because of the continuous evaporation process that cools the roof, the average decrease in the external surface temperature in the case of multiple water replenishment is 1.9 times that of the case of single water replenishment from 12:00-18:00, whereas the decrease in the accumulated internal surface heat flux is 1.5 times that of the case of single water replenishment from 12:00 to 18:00.

Table 5 Average cooling magnitude of external surface temperature and accumulated decrease magnitude of internal surface heat flux

water replenishing conditions	Average external surface temperature decrease (°C)			Accumulation internal surface heat flux decrease (W/m^2)		
	6:00-11:00	12:00-18:00	19:00-23:00	6:00-11:00	12:00-18:00	19:00-23:00
Single replenishing	0.0	2.9	0.1	0.0	43.5	19.3
Multiple replenishing	0.0	5.6	1.1	0.0	63.4	55.7

5 Conclusions and Discussions

In this study, non-linear multiple regression analysis was applied to determine a mathematical model to calculate the evaporation rate of a roof. The model adopted the surface solar absorptivity

and meteorological parameters as independent variables which can all be directly obtained from building energy simulation software. Thus, the software can conveniently adopt the model to calculate the evaporation heat transfer and avoid complicated and time-consuming iterative calculations. Although this mathematical model was based on specific roof structures and meteorological parameters (necessitating further studies to confirm its applicability to other roof structures and meteorological parameters), the development method of this mathematical model can provide a valuable reference for future studies.

Evaporation starting at different time reduces the external surface temperature and internal surface heat flux to different degrees. In the conditions studied here, when evaporation commenced at 7:00, 11:00, and 15:00, compared to the corresponding value of the no-evaporation roof, the highest external surface temperature were reduced by 0.6°C, 1.8°C, and 0°C, respectively; in addition, the accumulated internal surface heat flux from 16:00-20:00, which is the peak load period for residential buildings [24], were decreased by 6.1%, 10.8%, and 8.6%, respectively, which meant that the room cooling loads could also be accordingly reduced during that period.

By increasing the frequency of water replenishment, the evaporation process can be extended, and continuous evaporative cooling can therefore be achieved. In this article, when the evaporation layer was watered frequently, the accumulated internal surface heat flux from 16:00-20:00 was 21.2% less than that of the no-evaporation roof.

Although the timescale in this study is only 24 h, the results provide a reference for simulating building energy consumption on a longer timescale. Future research based on this study could include the following: adding a description of the building surface evaporation process to the software that dynamically calculates the building energy consumption and analysing the effects of the precipitation time (or water spray time) and precipitation amount (water spray amount) on building energy consumption, which could provide a passive technical method to design the net zero energy building and analyze the power demand response.

Acknowledgements

Nomenclature

b_1, b_2, b_3 constants

c specific heat (kJ/kg·K)

E evaporation amount per unit area (kg/m^2·h)

e_a actual vapor pressure (kPa)

e_s saturation vapor pressure (kPa)

G surface heat flux (MJ/m^2)

h_o external surface combined heat transfer coefficient (W/m^2·K)

h_i internal surface combined heat transfer coefficient (W/m^2·K)

I_s total shortwave radiation on the roof surface (W/m^2)

k number of layer

m number of time

q_s surface net shortwave radiation (W/m^2)

q_c surface combined heat transfer (W/m^2)

q_e surface evaporation heat transfer (W/m^2)

q_i heat flux on the interior surface of sample (W/m^2)

R_n surface net radiation (MJ/m^2)

T all-day average air temperature or hourly air temperature (°C)

t_e ambient air temperature (°C)

t_i indoor air temperature (°C)

t_s surface temperature (°C)

u all-day average wind speed or hourly wind speed (m/s)

α surface solar absorptivity

γ psychrometer constant (kPa/°C)

Δ slope of saturation vapor pressure curve (kPa/°C)

θ_e exterior surface temperature (°C)

θ_i interior surface temperature (°C)

λ thermal conductivity (W/m·K)

ρ density (kg/m^3)

τ time (s)

Reference

[1] Marszal, A. J., Heiselberg, P., Bourrelle, J. S., Musall, E., Voss, K., Sartori, I., & Napolitano, A. (2011). Zero Energy Building–A review of definitions and calculation methodologies. Energy and Buildings, 43(4), 971-979.

[2] Deng, S., Wang, R. Z., & Dai, Y. J. (2014). How to evaluate performance of net zero energy building–A literature research. Energy, 71, 1-16.

[3] Berry, S., Whaley, D., Davidson, K., & Saman, W. (2014). Near zero energy homes–What do users think?. Energy Policy, 73, 127-137.

[4] Favoino, F., Overend, M., & Jin, Q. (2015). The optimal thermo-optical properties and energy saving potential of adaptive glazing technologies. Applied Energy, 156, 1-15.

[5] Zhang R., Nie Y., Lam K. P., Biegler L. T. (2014). Dynamic optimization based integrated operation strategy design for passive night ventilation and active building air conditioning. Energy

and Buildings, 85,126–135.

[6] Sadineni, S. B., Madala, S., & Boehm, R. F. (2011). Passive building energy savings: A review of building envelope components. Renewable and Sustainable Energy Reviews, 15(8), 3617-3631.

[7] Dabaieh, M., Wanas, O., Hegazy, M. A., & Johansson, E. (2015). Reducing cooling demands in a hot dry climate: A simulation study for non-insulated passive cool roof thermal performance in residential buildings. Energy and Buildings, 89, 142-152.

[8] Kharrufa, S. N., & Adil, Y. (2012). Upgrading the building envelope to reduce cooling loads. Energy and Buildings, 55, 389-396.

[9] Sosa, L. C. H., & Gómez-Azpeitia, G. (2014). Cooling Average Potential of Evaporative Cooling System in Dry Warm Climate. Energy Procedia, 57, 2554-2563.

[10] Yang, W., Wang, Z., & Zhao, X. (2015). Experimental investigation of the thermal isolation and evaporative cooling effects of an exposed shallow-water-reserved roof under the sub-tropical climatic condition. Sustainable Cities and Society, 14, 293-304.

[11] Zhang, L., Liu, X., Meng, Q., & Zhang, Y. (2015). Experimental study on the impact of mass moisture content on the evaporative cooling effect of porous face brick. Energy Efficiency, 1-13.

[12] Zhang, L., Feng, Y., Meng, Q., & Zhang, Y. (2015). Experimental study on the building evaporative cooling by using the Climatic Wind Tunnel. Energy and Buildings, 104, 360-368.

[13] Wanphen, S., & Nagano, K. (2009). Experimental study of the performance of porous materials to moderate the roof surface temperature by its evaporative cooling effect. Building and Environment, 44(2), 338-351.

[14] Pires, L., Silva, P. D., & Castro Gomes, J. P. (2011). Performance of textile and building materials for a particular evaporative cooling purpose. Experimental Thermal and Fluid

Science, 35(4), 670-675.

[15] He, J., & Hoyano, A. (2009). A 3D CAD-based simulation tool for prediction and evaluation of the thermal improvement effect of passive cooling walls in the developed urban locations. Solar Energy, 83(7), 1064-1075.

[16] He, J., & Hoyano, A. (2010). Experimental study of cooling effects of a passive evaporative cooling wall constructed of porous ceramics with high water soaking-up ability. Building and environment, 45(2), 461-472.

[17] Chen, W., Liu, S., & Lin, J. (2015). Analysis on the passive evaporative cooling wall constructed of porous ceramic pipes with water sucking ability. Energy and Buildings, 86, 541-549.

[18] Karamanis, D., Kyritsi, E., & Krimpalis, S. (2015). Well-ordered nanoporous materials for low-temperature water phase changes and solar evaporative cooling. Solar Energy Materials and Solar Cells, 139, 34-43.

[19] Kaşka, Ö., & Yumrutaş, R. (2008). Comparison of experimental and theoretical results for the transient heat flow through multilayer walls and flat roofs. Energy,33(12), 1816-1823.

[20] People's Republic of China, national standard: thermal design code for civil building GB 50176-93, Ministry of Housing and Urban-Rural Development of the People's Republic of China, Beijing (1993).

[21] Davis, M. M., & Hirmer, S. (2015). The potential for vertical gardens as evaporative coolers: An adaptation of the 'Penman Monteith Equation'. Building and Environment, 92, 135-141.

[22] Zingre, K. T., Wan, M. P., Wong, S. K., Toh, W. B. T., & Lee, I. Y. L. (2015). Modelling of cool roof performance for double-skin roofs in tropical climate.Energy, 82, 813-826.

[23] Zainal, O. A., & Yumrutaş, R. (2015). Validation of periodic solution for computing CLTD (cooling load temperature difference) values for building walls and flat roofs. Energy, 82, 758-768.

[24] Turner, W. J. N., Walker, I. S., & Roux, J. (2015). Peak load reductions: Electric load shifting with mechanical pre-cooling of residential buildings with low thermal mass. Energy, 82, 1057-1067.